

Experimental investigation of drag reduction effects of polymer additives on turbulent pipe flow using ultrasound Doppler velocimetry

Şerife ZEYBEK VURAL, Göknuş BAYRAM, Yusuf ULUDAĞ*

Department of Chemical Engineering, Middle East Technical University, Ankara, Turkey

Received: 12.03.2013 • Accepted: 14.07.2013 • Published Online: 16.12.2013 • Printed: 20.01.2014

Abstract: Drag reduction in fully developed turbulent pipe flow with 4 concentrations (200 to 500 wppm or mg/kg) of low molecular weight sodium carboxymethylcellulose (CMC) in aqueous solutions was investigated experimentally. Drag reduction was determined by pressure drop measurements. Maximum drag reduction achieved was 22% using 500 wppm CMC solution. To observe the impact of the presence of CMC on the flow, ultrasound Doppler velocimetry (UDV) was employed to monitor the instantaneous velocity distributions. Experimental measurements were used to calculate Fanning friction factor and radial distributions of the axial time-averaged velocity, velocity fluctuation (turbulent intensity), and eddy viscosity. Two impacts of increasing CMC concentration on the flow field were observed. The first effect was the decrease in the mean velocity gradient, especially near the wall, with increasing polymer amount, which in turn gave rise to a lower friction factor or pressure drop. Furthermore, smaller eddy viscosities were obtained in the flow. The second impact of polymer addition was on the velocity fluctuation or turbulent intensity variation along the radial distribution. Presence of the polymer suppressed the velocity fluctuations near the wall while the intensity in the turbulent core region became stronger than in the case of lower or no polymer addition.

Key words: Ultrasound Doppler velocimetry, turbulent pipe flow, water soluble polymers, drag reduction

1. Introduction

Addition of small amounts (tens of parts per million by weight) of polymer to flow results in the reduction of skin friction in turbulent flows. This phenomenon is known as drag reduction and was discovered by Toms¹ in 1948; therefore, it is termed the Toms phenomenon. Since that time, interest in drag reduction has grown because of its wide range of industrial applications. Despite the large number of experimental and theoretical studies in this area over half a century, an exact mechanism explaining the phenomenon has not been yet obtained due to the complexity of its physics.

Various mechanisms of drag reduction have been proposed in the literature. The most common one is Lumley's theory. Lumley² emphasized that for turbulent flow, outside the viscous sublayer polymer chains are stretched by turbulence because of the increasing strain rate in the turbulence and this causes enhanced effective viscosity in the turbulent region. On the other hand, the viscosity in the viscous sublayer remains low. However, Lumley did not provide detailed experimental results or theoretical models supporting the mechanism. Therefore, Hinch,³ Landahl,⁴ and Ryskin⁵ proposed models to analyze the mechanism. According to Lumley, Hinch, Landahl, and Ryskin, the main source of drag reduction is the increase in the local effective viscosity of the flow due to a hydrodynamic interaction between polymer chains and flow. In their research, the elastic effect

*Correspondence: yuludag@metu.edu.tr

of dilute polymer solutions was not considered. Thus, De Gennes⁶ investigated the energy exchange between the kinetic and elastic energy in the core of the turbulent flow, far from the boundary. He concluded that the polymer effect at small scales (high frequencies) is not described by a viscosity, but by an elastic modulus. Flexible polymers in dilute solutions enhance the viscosity in slow flows, but in strong, rapidly varying, shear fields, they behave elastically. A turbulent cascade (from large to small scales) should thus be deeply modified when the elastic stresses become comparable to the Reynolds stress. Den Toonder et al. investigated the roles of stress anisotropy and elasticity in the mechanism of drag reduction by polymer additives.⁷ The investigation was carried out by means of direct numerical simulation (DNS) and laser Doppler velocimetry (LDV). In DNS 2 different models were used. The first model was based on the viscous anisotropic effects, while the second one was an extension of the first model with an elastic component. They claimed that viscous anisotropic stresses introduced by extent of polymers play a key role in the mechanism of drag reduction.

In experimental studies, different kinds of flow measurement instrument have been used to observe drag reduction. Virk et al. employed a hot-wire anemometer to measure the turbulent intensities and energy spectrum.⁸ They reported that the technique was unreliable due to flow disturbances associated with the presence of hot wires in the flow. To observe strange turbulent fields that occurred under the conditions yielding a high degree of drag reduction, Warholic et al.⁹ used particle-image velocimetry (PIV), while Tamano and Itoh¹⁰ employed both PIV and LDV. Applicability to transparent media and restrictions in the flow geometry sizes are the most crucial limitations encountered generally in flow visualization techniques. LDV has been a powerful technique to investigate many aspects of fluid flow including drag reduction phenomena.^{7,10–12} Although LDV provides excellent temporal velocity measurements, in addition to the limitations encountered in flow visualization techniques, its single point measurement but not the entire flow field simultaneously can be a serious drawback for some applications.

The objective of the present study was to investigate drag reduction effects of polymers in turbulent flows via ultrasound Doppler velocimetry (UDV), which is a noninvasive and nondestructive and relatively new technique employed in flow measurements.^{13,14} UDV also provides a velocity profile in seconds as opposed to single point measurement methods like LDV. Its relatively low cost and ease of use are other considerable advantages over the other aforementioned measurement techniques. The results obtained in this study highlighted these benefits in spite of some of its current limitations associated with the poor signal-to-noise ratio in the regions close to the conduit walls.

2. Experimental

2.1. Experimental set-up and material

The experiments were carried out using the recirculation flow system shown in Figure 1. The flow system consists of a test section that is 6 m of polyvinylchloride (PVC) tubing with 46 mm inner diameter, connection plastic tubing, an in-line flow meter, valves, 2 plastic tanks, and a pump (Iwaki Magnet Pump, Japan). A constant water head is maintained by pumping the solution from the lower tank to the upper one. Both the overflow from the upper tank and the return flow from the experimental section are received in the lower tank. The constant head allowed operation at a steady average flow rate. The pressure drop measurements were taken over a 6-m long PVC pipe with a length of 1.0 m provided from the entry (to avoid entry problems) and 1.0 m from the exit by a U tube manometer with chloroform (CHCl_3). The distance between the pressure taps is 4 m.

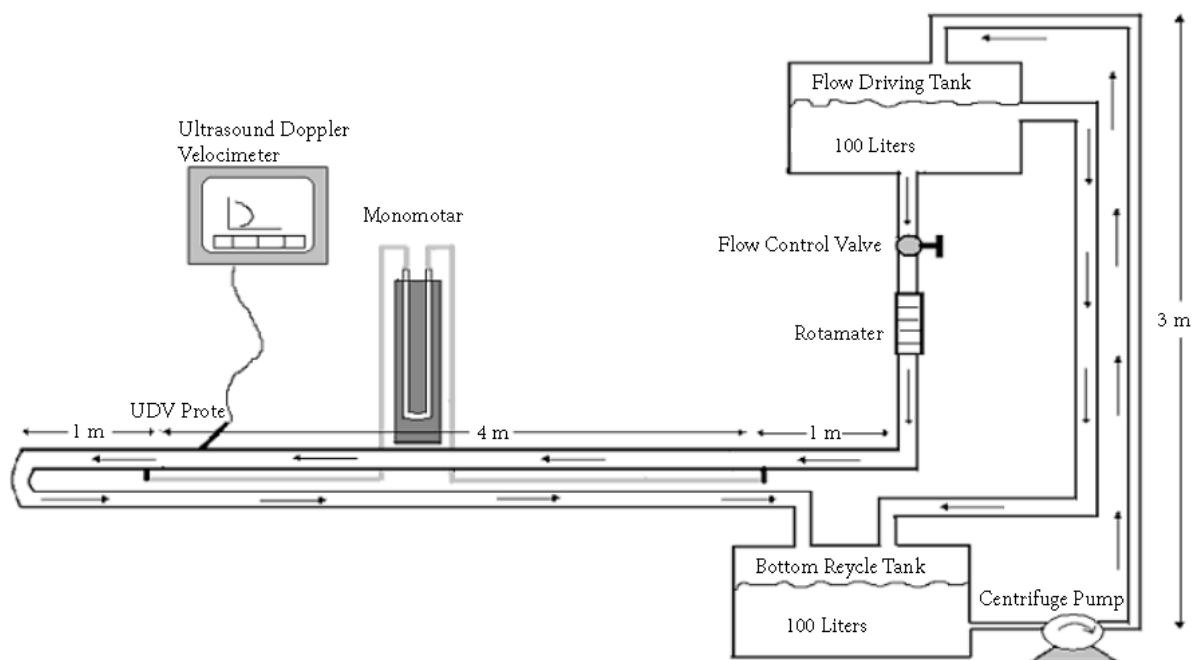


Figure 1. Experimental set-up.

Experiments were carried out with aqueous solutions of sodium carboxymethylcellulose (CMC) supplied by SIGMA Chemical Company. Properties of the CMC are given in Table 1. For the experimental study, polymers were dissolved in tap water. First, the tanks were filled with 138 L of water. Next, 28 g of CMC was dissolved in 2 L of water and the solution was stirred for 2 h using a stirring vessel (Servodyne Mixer, Cole-Palmer). Then the concentrated CMC solution was added to the tanks so that 200 wppm CMC solution was obtained. Other concentrations (300, 400, 500 wppm) were prepared by adding CMC to this solution. Before the experiments, polymer solutions were allowed to stand for 12 h at room temperature and during this time the covers of tank were closed to prevent evaporation. Then the solutions were characterized by density (calculated from mass and volume measurements) and viscosity (HAAKE Viscotester VT-01, Germany) measurements at room temperature. The results are given in Table 2. At the studied range of the CMC concentration, the shear thinning effect can be expected to be negligible. In an earlier study on the viscosity properties of CMC solutions, no significant change in the solution viscosity was observed until shear rates of 10 s^{-1} in the case of 1% CMC solution.¹⁵ This value is 20 times higher than the highest concentration in this study.

Table 1. Properties of sodium carboxymethylcellulose.

Molecular weight	Viscosity of 1% aqueous solution	Sodium content	Purity	Appearance
700 kDa	1.5 to 3.0 Pa s	8%	99.5%	White to yellow powder

Table 2. Physical properties of sodium carboxymethylcellulose solutions at room temperature.

	Water	200 wppm	300 wppm	400 wppm	500 wppm
Density, kg/m^3	980	983	983	985	985
Viscosity, Pa s	1×10^{-3}	1.2×10^{-3}	1.35×10^{-3}	1.65×10^{-3}	1.8×10^{-3}

The desired flow rate was established in the pipe using the flow control valve and the rotameter. Pressure drop was also recorded simultaneously by means of the manometer. Velocity profile measurements were obtained using the UDV system. The presence of tiny particles or scatterers helps to improve the signal-to-noise ratio of the measurements. Thus 12 g of Griltex 2A P1 copolyamide particles (EMS-Griltech, Switzerland) were added to the solution. Having average diameter of 3 μm in liquid, the particles did not lead to any appreciable diffraction of the ultrasonic beam with wavelength 372.5×10^{-6} m, around 3 μm . A container was designed to place the ultrasonic probe on the PVC pipe and it was filled with coupling liquid (water) to reduce refraction of the ultrasonic waves. The angle between the ultrasonic probe and pipe was 70° . The ultrasonic probe (TR0405LS) used for the experiments had 4-MHz frequency with 5-mm diameter and 90-mm length.

2.2. Flow quantities and turbulence measurements

The basic quantities measured for this experimental study are volumetric flow rate, pressure drop, and the velocity profiles. The Reynolds number used in the calculations is defined as

$$Re = \frac{DV_{av}\rho}{\mu}, \quad (1)$$

where D , V_{av} , ρ , and μ are pipe diameter, bulk average velocity, fluid density, and viscosity, respectively. For a fully developed turbulent flow, the relation between mean stress at the wall and axial pressure drop is provided by

$$\tau_w = \frac{D \Delta P}{4 \Delta x}. \quad (2)$$

The Fanning friction factor can be written as

$$f = \frac{\tau_w}{\frac{1}{2}\rho V_{av}^2}. \quad (3)$$

The amount of drag reduction, DR, is expressed as the wall shear stress difference between the solvent (water), τ_s , and the polymer solutions, τ_p , at the same Reynolds number,

$$DR\% = \frac{(\tau_s - \tau_p)}{\tau_s} \times 100 \quad (4)$$

The friction velocity

$$U^* = \sqrt{\frac{\tau_w}{\rho}} \quad (5)$$

and nondimensional velocity is

$$u^+ = \frac{U}{U^*}, \quad (6)$$

where U is pointwise time average velocity. In order to make the distance from the wall, y , dimensionless the following equation is used:

$$y^+ = \frac{U^*y\rho}{\mu}. \quad (7)$$

The root-mean-square velocity fluctuation is defined as

$$u'_{rms} = \sqrt{u'^2}. \quad (8)$$

Eddy viscosity data are derived from the velocity profile and flow measurements. Total shear stress calculated using the pressure drop measurements is

$$\tau = \tau_v + \tau_t, \quad (9)$$

where τ is total local shear stress, τ_v is the viscous shear stress, and τ_t is the turbulent shear stress.

$$\tau = (\mu + \varepsilon) \frac{dU}{dr}. \quad (10)$$

Eq. (10) is denoted as a Boussinesq relation where μ is the dynamic viscosity of the solution and ε is the eddy viscosity; in this way, eddy viscosity values are calculated at each radial position.

3. Results and discussion

In the experiments, drag reduction was determined by pressure drop measurements in fully developed turbulent pipe flow along the pipe. In order ensure that pressure taps are in the fully developed flow region, entry length, l_e , is checked through the following empirical relation:

$$\frac{l_e}{D} = 4.4 (Re)^{1/6}. \quad (11)$$

For the highest Re around 20,000 and pipe diameter of 4.6 cm, l_e becomes 105 cm. That distance is very close to the 100-cm distance between the pipe ends and the pressure taps.

Plots of the friction factor versus Reynolds number obtained at different polymer concentrations are shown in Figure 2. The graph shows the level of drag reduction for each polymer solution. At each polymer concentration friction factor decreases as Re gets higher and then it becomes constant with respect to Re. Since there is no drag reduction in laminar flow, friction factors at different polymer concentration converge to the same value as Re decreases. The effect of polymer concentration on the drag reduction appears in the form of a lower friction factor at any Re value. In the figure it is obvious that high polymer concentration yields higher drag reduction and that becomes more and more pronounced in highly turbulent flows. Also included in Figure 2 are the Prandtl–Karman law (the law of the wall) and MDR curves. The data for the water are in good agreement with the Prandtl–Karman law, which is the uppermost line. In their experiments, Pinho and Whitelaw used carboxymethylcellulose solutions at 1000, 2000, 3000, and 4000 wppm concentrations.¹⁶ They observed MDR in 2000 wppm CMC solution. In our study, however, the concentrations of CMC solutions are not high enough to reach the MDR asymptote. Our primary objective was to investigate drag reduction itself. In order to avoid possible complications associated with the high polymer concentrations around MDR, 500 wppm was chosen as the maximum CMC concentration in the experiments.

The effect of Reynolds number for each polymer solution on drag reduction is given in Figure 3. Drag reductions were obtained using Eq. (4). Figure 3 depicts that higher drag reductions are achieved when the polymer concentration is increased. Drag reduction becomes even higher at high Re numbers. In the experiments, the maximum drag reduction achieved was 22% using 500 wppm CMC solution, which is a considerable value compared to those reported in the literature. For example, Pinho and Whitelaw reported 46.8% drag reduction at 1000 wppm CMC solution at Re number 17,000.¹⁶ It should be noted that both the

concentration and Re values were higher than the values used in this study and so higher drag reduction was observed in the reported study.

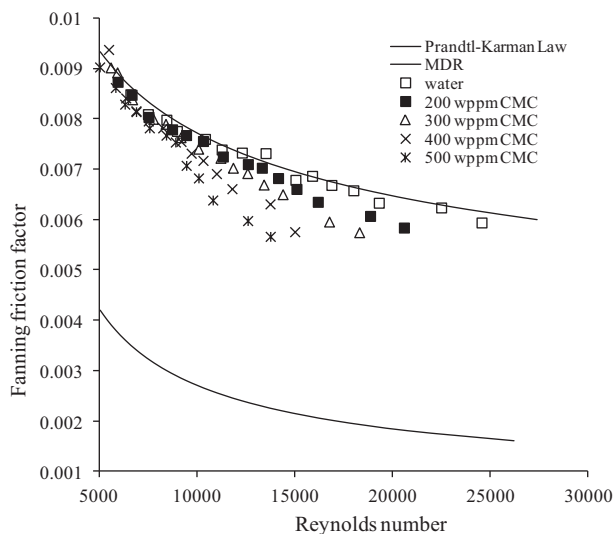


Figure 2. Fanning friction factor versus Reynolds number.

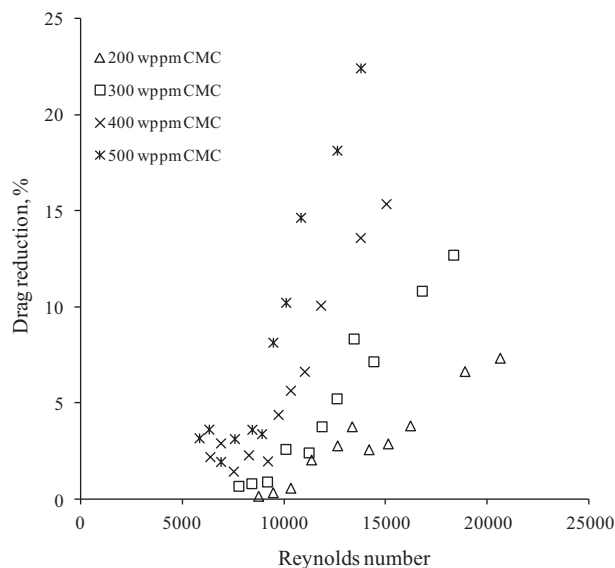


Figure 3. Drag reduction versus Reynolds number at various concentrations of CMC solutions.

Figure 4 shows the drag reduction values with respect to CMC concentration at the same bulk average velocity, V_{av} , of 0.55 m/s. As expected, drag reduction increases with the addition of polymer to the solution. That increase can be approximated by a linear relation within the studied range of CMC concentration as shown in the figure. The drag reductions versus polymer concentration characteristics are consistent with those published earlier.^{16,17} In those reports, an increase in polymer consideration gave rise to stronger viscoelastic properties that in turn resulted in higher drag reduction.

The results obtained so far clearly demonstrate that higher drag reductions can be attained as polymer concentration and Re are increased. The results, on the other hand, do not provide any direct clue to the mechanisms of drag reduction. To answer the question of how drag reduction occurs, the impact of polymer addition on the turbulent flow field should be determined. Therefore, in this study, a new flow measurement technique, UDV, was used to obtain both time-averaged and fluctuating velocity distributions within the pipe simultaneously with pressure drops. It should be noted that gathering the entire velocity profile data took a very short time, less than 20 ms.

Time averaged velocity, U , profiles obtained at different polymer concentrations using UDV are depicted in Figure 5. The vertical axis represents normalized time-averaged velocity, while the horizontal axis is normalized radial position. The time average velocity data at the center of the pipe, U_o , and pipe radius R were used to scale the velocity and position, respectively. In the figure all velocity profiles exhibit typical characteristics of time-averaged velocity distribution in a turbulent flow. Little velocity variation in the core and a high velocity gradient near the wall are observed. Addition of polymer has small impact on the core region, while it decreases the velocity gradient near the wall appreciably. Therefore, the highest gradient is observed in the case of water flow without polymer. It decreases with increasing polymer concentration. It is well known that degree of momentum interaction between the wall and flow is directly dependent on that gradient. Hence, lower velocity gradient in the case of flow with polymer gives rise to lower shear stress or drag.

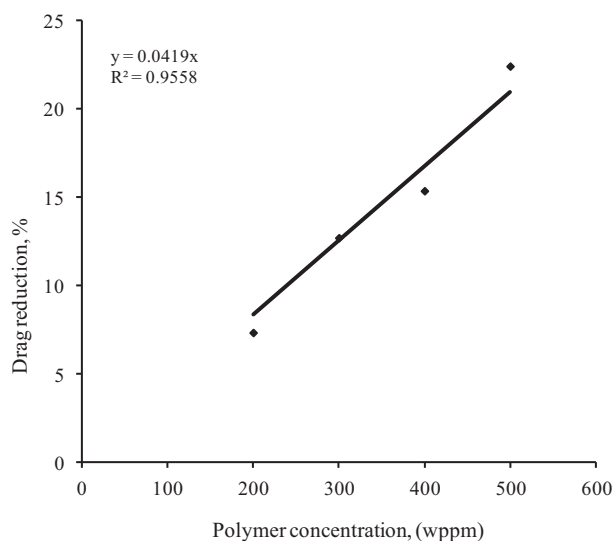


Figure 4. Drag reduction versus polymer concentration.

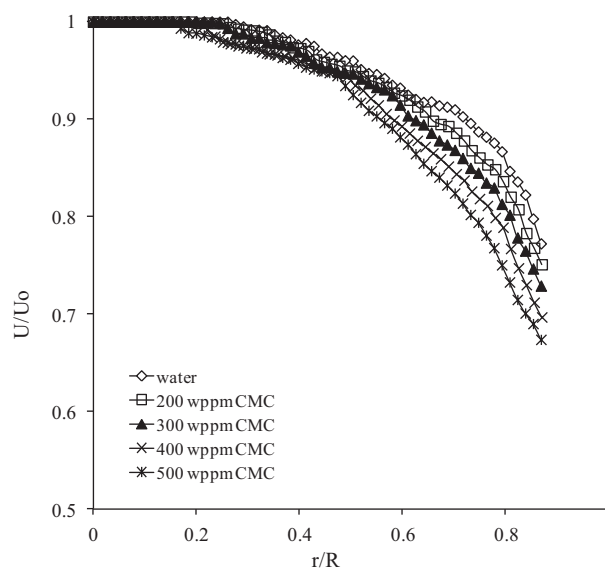


Figure 5. Mean axial velocity profiles at various concentrations of CMC solutions.

The closest velocity measurement to the wall was achieved at 3 mm from the wall. This distance corresponds to the logarithmic sublayer under the flow conditions of the experiments. Due to the resolution limitations and negative interactions with the pipe wall velocity data could not be obtained in the regions closer to the wall where the viscous sublayer occurs. Unfortunately, important hydrodynamic interactions between turbulent flow and the solid surfaces are mostly confined to this region. Nevertheless, the results obtained in the outer regions have many crucial implications regarding the turbulence and drag reduction characteristics as reported below.

To observe the behavior of polymer in the turbulent boundary layer, the typical velocity profile for turbulent boundary layer has to be shown. In Figure 6 the universal nondimensional mean velocity profiles are plotted as a function of nondimensional radial distance from the wall. Velocities are nondimensionalized using friction velocity. This figure also includes several velocity curves; the Prandtl–Karman law (the Newtonian wall law) profile, the viscous sublayer profile, and MDR. The velocity data at low values of y^+ could not be obtained; therefore, a comparison between the results of this study and the literature cannot be done in the viscous and buffer sublayer. In Figure 6 the slope of the profiles increases with polymer concentration since high polymer concentrations yield lower wall shear stresses and hence lower friction velocities, which are used to scale the velocities in the figure. According to Den Toonder et al. the buffer layer is thickened due to polymer additives and this causes an upward shift of the logarithmic profile.⁷

The effect of CMC addition on the logarithmic layer is investigated by obtaining turbulence intensities using UDV data. The variation in the axial root-mean-square velocity fluctuation with the dimensionless radial distance from the pipe center is shown in Figure 7. Turbulent intensities show the characteristic behavior for the drag reduced flow. For polymer concentrations, with the exception of 200 wppm CMC, the height of the peak increases with respect to water and the peak shifts away from the wall for 300, 400, and 500 wppm CMC solutions to a lower r/R value. The height of the peak increases with addition of polymer. This sudden increase shows that the turbulent energy of the axial velocity near the wall is transported from small scales to large scales. The change is largest when the r/R value is 0.9 corresponding to the logarithmic sublayer. This result is consistent with the shift of the logarithmic sublayer in the axial mean velocity profile. Therefore, it is seen that

polymers suppress the turbulence by decreasing its energy near the pipe wall. These results are qualitatively consistent with those published earlier.^{7,9} The observations suggest that anisotropy of the stress field in the flow derives the drag reduction mechanism associated with the polymer addition.

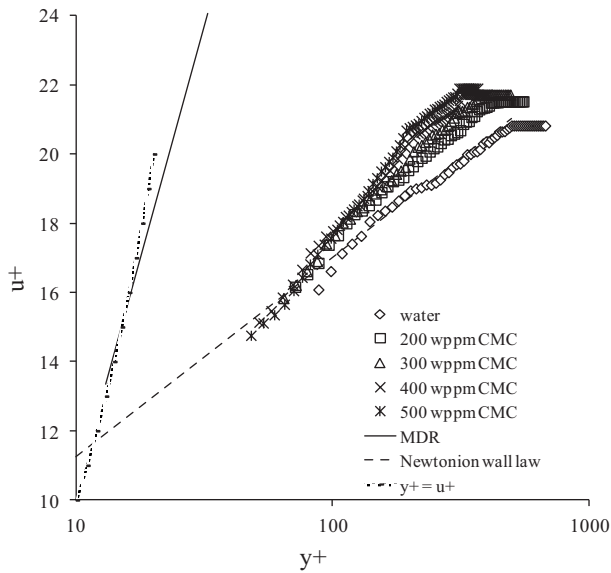


Figure 6. Mean axial velocity profiles at various concentrations of CMC solutions in terms of wall units.

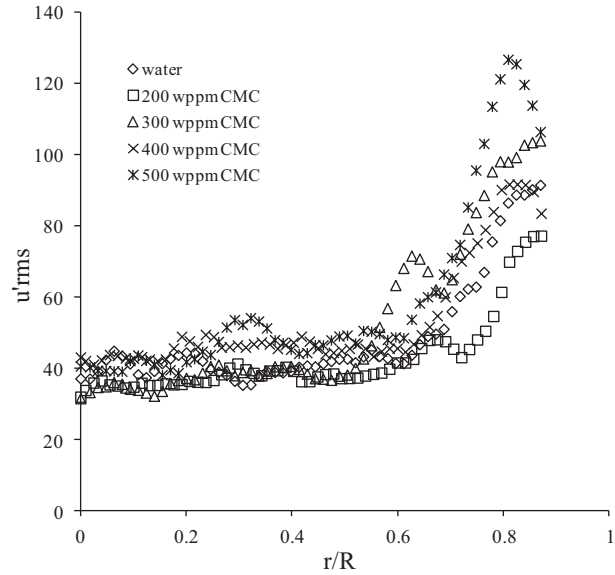


Figure 7. Mean axial turbulence intensity profiles.

Eddy viscosity profiles during the drag reduction are given in Figure 8. They were derived from velocity profile and flow measurements. The eddy viscosity through the pipe radius is decreased by adding polymer. Near the pipe wall it takes the lowest value. The results depicted in Figures 5 and 8 together provide an insight into the total momentum flux and hence drag reduction. When the velocity gradient near the pipe wall is

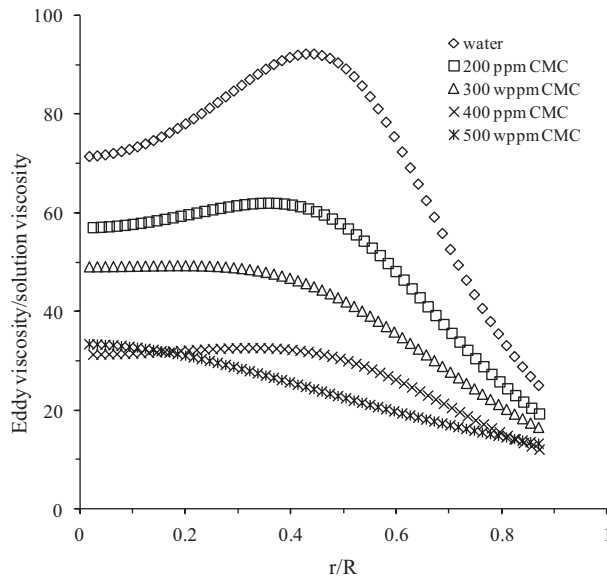


Figure 8. Nondimensional eddy viscosity profiles.

considered, its highest value occurs in the case of water and it gets lower as the polymer concentration increases as explained earlier. Despite the lack of velocity data very close to the pipe wall ($r/R > 0.87$), this tendency in the velocity gradient seems to be outweighing the increase in the solution viscosity due to the addition of polymer. For example, viscosity increases from 1 cP to 1.8 cP in the case of 500 wppm polymer addition. In the core regions it is the fluctuations in the velocity or Reynolds stresses that mainly derive the momentum transfer. A considerable decrease in eddy viscosity with the addition of polymer in Figure 8 indicates that momentum flux or shear stress gets lower as polymer concentration increases due to suppression of the turbulence by the polymer chains. These findings are in parallel with those reported by Virk.¹⁸

4. Conclusions

Through the experimental results, the following conclusions can be drawn.

1. High polymer concentration yields higher drag reduction and that becomes more pronounced in highly turbulent flows.
2. Addition of polymer has a small impact on the core region of the time averaged velocity profile, while it decreases the velocity gradient near the wall appreciably.
3. Polymer addition suppresses the turbulence by decreasing its energy near the pipe wall.
4. The eddy viscosity across the pipe cross section decreases in the presence of polymer molecules.
5. The turbulence measurements near the wall for 46 mm inside diameter pipe using UDV proved very difficult, while reliable velocity data in the turbulent core region could be obtained. Using a larger diameter pipe can be helpful in terms of enhanced pipe wall region measurements.

Acknowledgment

This study was supported by the Scientific and Technological Research Council of Turkey through the grant MISAG-232.

References

1. Toms, B. A. In Proceedings of the First International Congress of Rheology, Scheveningen, Holland, 21–24 September 1948; Burgers, J. M., Ed; North Holland, Amsterdam, 1949, pp. 135–141.
2. Lumley, J. L. *J. Polymer Sci.: Macromol. Rev.* **1973**, *7*, 263–290.
3. Hinch, E. J. *Phys. Fluids* **1977**, *20*, S22–S30.
4. Landahl, M. T. *Phys. Fluids* **1977**, *20*, S55–S63.
5. Ryskin, G. *Phys. Rev. Lett.* **1987**, *59*, 2059–2062.
6. De Gennes, P. G. *Physica A* **1986**, *140*, 9–25.
7. Den Toonder, J. M. J.; Hulsen, M. A.; Kuiken, G. D. C.; Nieuwstadt, F. T. M. *J. Fluid Mech.* **1997**, *337*, 193–231.
8. Virk, P. S.; Merrill, E. W.; Mickley, H. S.; Smith, K. A. *J. Fluid Mech.* **1967**, *30*, 305–328.
9. Warholic, M. D.; Heist, D. K.; Katcher, M.; Hanratty, T. J. *Exp. Fluids* **2001**, *31*, 474–483.
10. Tamano, S.; Itoh, M. *J. Turbulence* **2011**, *12*, 1–22.
11. Ptasiniski, P. K.; Nieuwstadt, F. T. M.; Van Den Brule, B. H. A. A.; Hulsen, M. A. *Flow Turbul. Combust.* **2001**, *66*, 159–182.

12. Japper-Jaafar, A.; Escudier, M. P.; Poole, R. J. *J. Non-Newton. Fluid.* **2009**, *161*, 86–93.
13. Dogan, N.; McCarthy, M. J.; Powell, R. L. *Meas. Sci. Technol.* **2005**, *16*, 1684–1690.
14. Köseli, V.; Zeybek, Ş.; Uludag, Y. *Turk. J. Chem.* **2006**, *30*, 297–305.
15. Yang, X. H.; Zhu, W. L. *Cellulose* **2007**, *14*, 409–417.
16. Pinho, F. T.; Whitelaw, J. H. *J. Non-Newton. Fluid.* **1990**, *34*, 129–144.
17. Escudier, M. P.; Presti, F.; Smith, S. *J. Non-Newton. Fluid.* **1999**, *81*, 197–213.
18. Virk, P. S. *AIChE J.* **1975**, *21*, 625–656.